Experimental Investigation of Air-Sea Transfer of Momentum and Enthalpy at High Wind Speed

By: Moshe Alamaro[1], Kerry A. Emanuel[1], Wade R. McGillis[2]
[1] *Department of Earth, Atmospheric and Planetary Sciences, Massachusetts Institute of Technology;*
[2] *Woods Holes Oceanographic Institution.*

Abstract. Thermodynamic analysis and numerical modeling of hurricane intensity has shown that it is sensitive to enthalpy and momentum transfer from the ocean surface. Direct measurements of drag are not easily performed on the high seas. Therefore, an annular wind wave tank has been constructed in which aspects of a tropical storm boundary layer were simulated. The air velocity inside the annular tank is comparable to that of a hurricane.

This paper focuses mainly on the design and engineering of the tank, the fluid mechanics of the rotational flow in the tank using angular momentum analysis, the design of experiments, and experimental results. It provides experimental data on drag and latent, sensible and total enthalpy transfer at high air speed relative to the moving water surface. The design of the wind-wave tank and the experiments create a foundation for future and more comprehensive high air speed experimental programs using a linear tank.

Key Words: Air-sea interaction, spray, tropical cyclones, heat and momentum transfer.

1. Experimental Apparatus and introduction

A circular wind wave tank made of two acrylic concentric walls was constructed, as shown in Figures 1 and 2. The water height can be varied in the annulus. A windvane, powered by a 1 kW electric motor, moves the air over the water surface. The shear over the water surface propels the water. An Acoustic Doppler Velocitmeter (ADV) measures the water velocity. An anemometer measures the air velocity. The tank is equipped with an adjustable false bottom that enables the distance from the windvane paddle to the water surface to be varied for the same depth of water. The tank is also equipped with apparatus to conduct enthalpy transfer experiments. All the experiments used Poland Spring™ water to minimize variations in water properties.

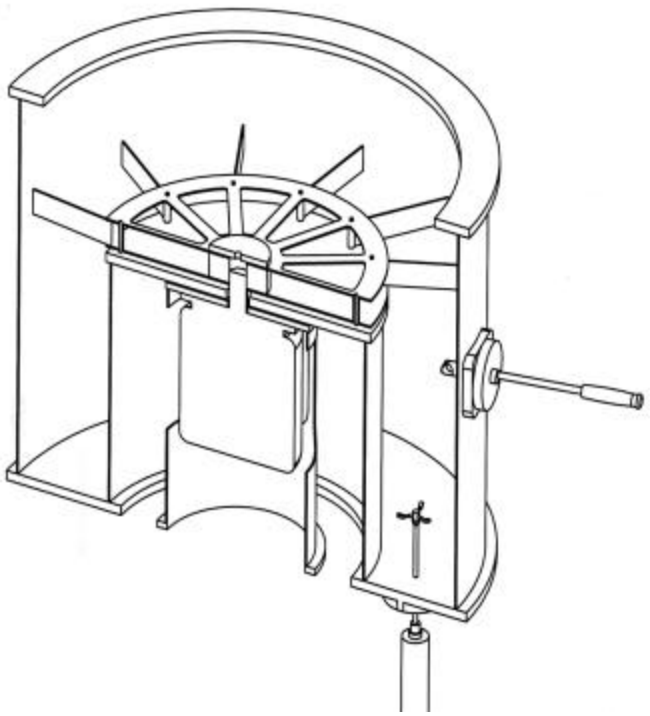

Figure 1: 3-D view of the annular wind wave tank. The outer and inner radiuses are $r_0 = 0.479\ m$ and $r_{in} = 0.284\ m$ respectively.

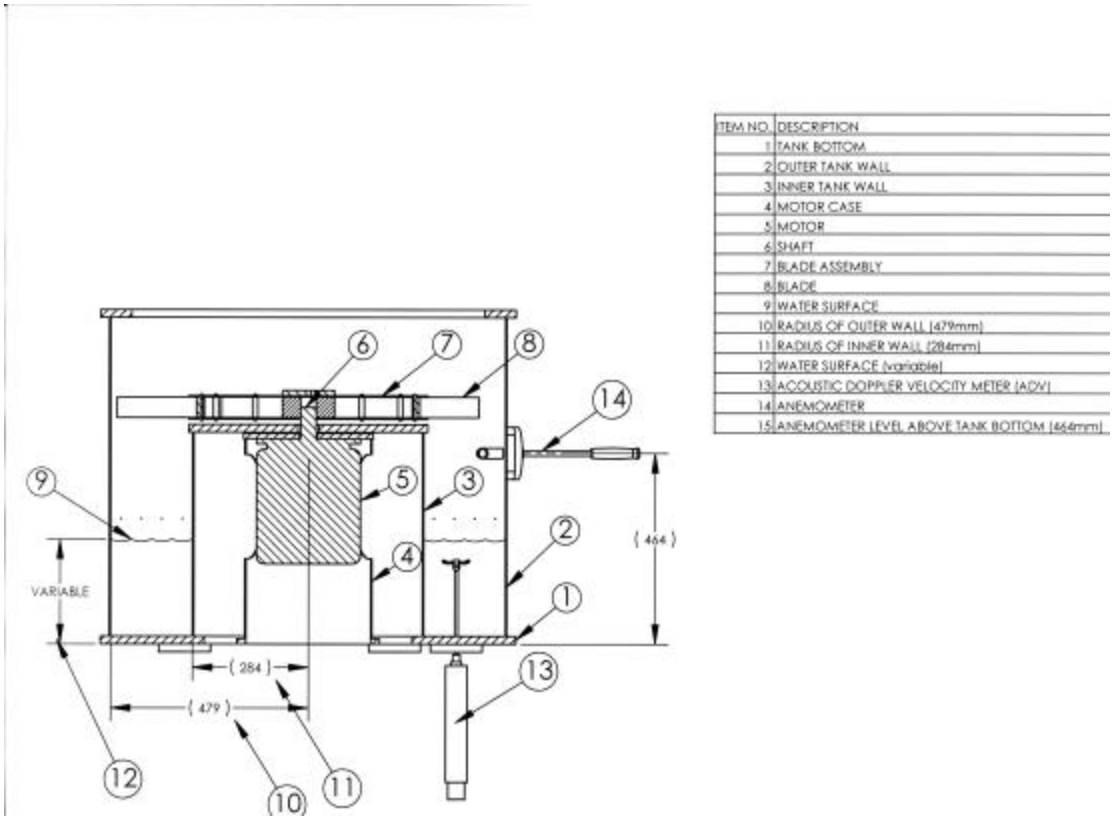

Figure 2: Cross section of wind wave tank and dimensions

The rate of input of available energy into a hurricane from the ocean surface per unit area of the ocean below the storm is:

$$G = hC_k \rho_a V_s (k_o^* - k_a) \quad (1)$$

Where G stands for energy generation, C_k is a dimensionless enthalpy transfer coefficient that accounts for both the latent and sensible heat transfers, V_s is the surface wind speed at a specified height above the water surface, k_o^* and k_a are the enthalpies of the ocean surface and the atmosphere respectively, and h is the heat engine cycle efficiency of the storm system. Bistre & Emanuel (1998) and Alamaro (2001) used both a Second Law analysis and dynamics to show that:

$$h = \frac{T_s - T_0}{T_0} \quad (2)$$

Where $T_s \approx 300K$ is the ocean surface temperature during the storm and $T_0 \approx 200K$ is the typical storm outflow temperature, so h is the hurricane "Carnot heat engine" efficiency, is approximately 0.5.

For fully developed hurricane when the storm intensity is steady, the generation energy given by (2) is balanced by dissipation over the sea surface. The approximated rate of dissipation per unit area is given by:

$$D = C_D \rho_a V_s^3 \quad (3)$$

Where C_D is the drag coefficient. Equating the generation and dissipation given by (1) and (3):

$$V_s^2 = h \frac{C_k}{C_D} (k_o^* - k_a) \quad (4)$$

We are interested in the maximum of V_s, which is in the vicinity of the eye wall. The magnitudes of h and $(k_o^* - k_a)$ in the vicinity of the eye wall can be estimated from observations of the storm environment. Emanuel (1986, 1988) has shown in a more rigorous analysis that indeed the maximum azimuthal wind speed varies as $\left(\frac{C_k}{C_D}\right)^{\frac{1}{2}}$ where C_k is the exchange coefficient of both latent and sensible heat and C_D is the surface drag coefficient.

The actual values of C_k and C_D as a function of wind speed cannot be deduced from similarity between momentum, energy and species concentration equations over the agitated ocean surface, as could be done over a flat surface. On the other hand, direct measurements of drag, evaporation, and sensible heat transfer are not easily performed on the high seas. Therefore, the goal of this investigation is to estimate magnitudes of C_D and C_k as a function of wind speed over the water surface using a laboratory apparatus.

2. Angular momentum and shear stress analysis

2.1 Basic Formulation

The drag coefficient over the ocean surface is defined as:

$$C_D = \frac{t_s}{r_a V_{10}^2} \tag{5}$$

Where t_s is the shear stress over the water surface, r_a is the air density and V_{10} is the air velocity at a reference height of 10 meters. The following is a simplified model that enables the simulation, measurement, and calculation of the shear stress t_s over the water surface in the wind wave tank. The model uses angular momentum motion equations for the rotating water mass, which is treated as a rigid body.

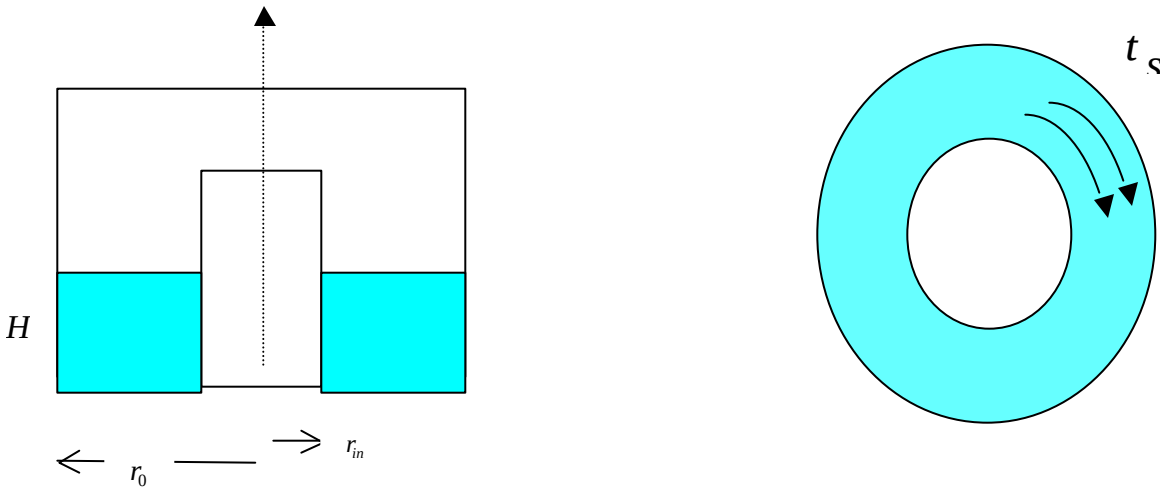

Figure 3: Side and upper views of the wind wave tank. Air motion over the water surface results in a propelling shear stress τ_s and propelling torque T_{propel}.

We assume that the water in the tank is in rigid body rotation. We assume also that the propelling shear stress is not a function of the radius: $\tau_s \neq \tau_s(r)$. The differential propelling torque provided by the stress applied to a differential water surface area $dA = r\,dq \cdot dr$ is:

$$dT_{propel} = \tau_s\, dA\, r \tag{6}$$

The entire propelling torque is:

$$T_{propel} = \int_{r_{in}}^{r_0} \int_0^{2p} \tau_s\, dA\, r = \int_{r_{in}}^{r_0} \int_0^{2p} \tau_s\, r\, dq \cdot dr\, r = \frac{2}{3} p \left(r_0^3 - r_{in}^3\right) \cdot \tau_s \tag{7}$$

The outer, inner, and bottom walls provide a retarding torque T_{retard} through shear stresses.

The total torque on the rigid body rotating water mass is then:

$$T_{total} = T_{propel} + T_{retard} \tag{8}$$

The angular momentum of a differential water mass assuming rigid body rotation with angular velocity Ω is:

$$dM = r_w \ (r\,dq\ dr\ dz)\,(\Omega r)\,r \tag{9}$$

where r_w is the water density. The total angular momentum of the water mass is thus:

$$M = r_w \int_0^H dz \int_0^{2p} dq \int_{r_{in}}^{r_0} r^3 dr = \frac{p}{2}\, r_w\, H\left(r_0^4 - r_{in}^4\right)\Omega \tag{10}$$

where H is the water depth. To derive the equation of angular motion we use the fact that the rate of change of the angular momentum is equal to the total applied torque:

$$\frac{\partial M}{\partial t} = \frac{p}{2}\, r_w\, H\left(r_0^4 - r_{in}^4\right)\frac{\partial \Omega}{\partial t} = T_{propel} + T_{retard} \tag{11}$$

In steady state: $\dfrac{\partial M}{\partial t} = 0$ and $T_{propel} = -T_{retard}$ (12)

2.2 Propelling torque and stress

The procedure for measuring and calculating the propelling torque and stress is as follows: First bring the water mass to a steady state rigid body rotation for certain V_s - the relative air velocity over the moving water surface. Second cut the power of the electric motor. With no

wind the stress imparted to the water surface is eliminated. The equation of motion just after the power cut at $t = 0$ when there is no propelling stress and torque is:

$$\frac{\partial M}{\partial t} = \frac{1}{2}\rho r_w H\left(r_0^4 - r_{in}^4\right)\frac{\partial \Omega}{\partial t} = -T_{retard} = +T_{propel} \tag{13}$$

Measuring $\frac{\partial \Omega}{\partial t}$ just after spindown starts will enable determining the propelling torque and the propelling shear stress. By combining (15) with (9) we get:

$$T_{propel} = \frac{2}{3}\rho\left(r_0^3 - r_{in}^3\right)\cdot t_s = -\frac{1}{2}\rho r_w H\left(r_0^4 - r_{in}^4\right)\frac{\partial \Omega}{\partial t} \tag{14}$$

and the surface shear stress is:

$$t_s = -\frac{\frac{1}{2}\rho r_w H\left(r_0^4 - r_{in}^4\right)\frac{\partial \Omega}{\partial t}}{\frac{2}{3}\rho\left(r_0^3 - r_{in}^3\right)} = -\frac{3}{4} r_w H \frac{\left(r_0^4 - r_{in}^4\right)}{\left(r_0^3 - r_{in}^3\right)}\frac{\partial \Omega}{\partial t} \tag{15}$$

To obtain $\frac{\partial \Omega}{\partial t}$ of the water mass, the velocity of the water V_w is measured at a distance R_D (the location of the ADV) from the tank center so that: $\frac{\partial \Omega}{\partial t} = \frac{1}{R_D}\frac{\partial V_w}{\partial t}$. Substituting into (15):

$$t_s = -\frac{3}{4} r_w \frac{H}{R_D}\frac{\left(r_0^4 - r_{in}^4\right)}{\left(r_0^3 - r_{in}^3\right)}\frac{\partial V_w}{\partial t} \tag{16}$$

The deceleration of the water mass $\frac{\partial V_w}{\partial t}$ is obtained by spindown experiments that are described in later sections.

2.3 Parabolic Shape Factors

Due to the centrifugal acceleration, the water surface will not be horizontal. The water surface becomes parabolic in r or $H = H(r)$. Therefore, the definition of z_a , the height above the water surface where air velocity is measured is compromised. The water surface area and the water moment of inertia are also changed.

Consider rigid body rotation of the water mass. Equilibrium in the r direction at any point in the water gives:

$$\frac{dp}{dr} = -r\frac{V^2}{r} = -r\ \Omega^2\ r \quad \text{or} \quad \frac{dp}{dr} = \frac{dp}{dz}\frac{dz}{dr} = -r\ g\frac{dz}{dr} = -r\ \Omega^2 r \qquad (17)$$

Integrating gives:

$$\Delta z(r) = \frac{\Omega^2}{2g}\left(r^2 - r_{in}^2\right) \qquad r \geq r_{in} \qquad (18)$$

Using $\Omega = \frac{V_w}{R_D}$ and substituting the values for R_D, r_0 and r_{in}, equation (18) provides the height difference of the water surface between the outer water and inner walls for the specific geometry of the tank:

$$\Delta z = 0.0528\, V_w^2 \qquad (19)$$

Where V_w is in m s^{-1}

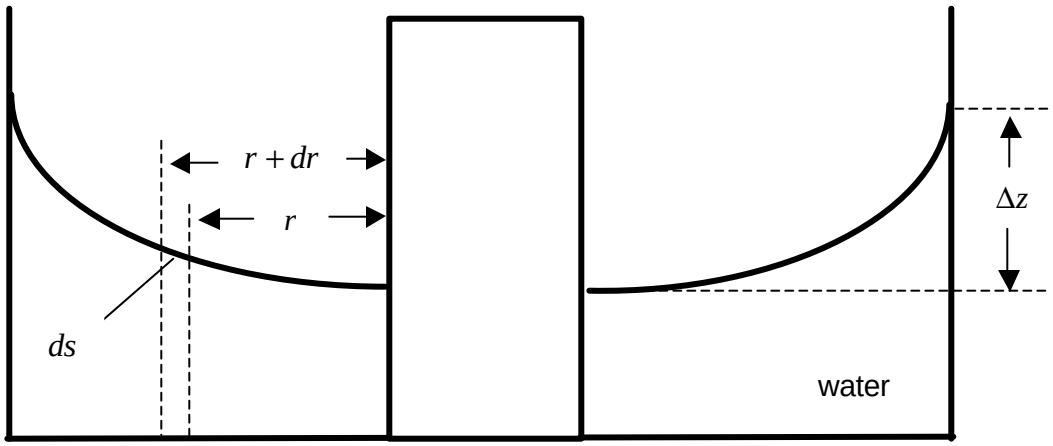

Figure 4: Parabolic surface of rotating rigid body water mass

The differential surface area in the rotating system is:

$$dA = ds\ 2p\ r \quad \text{or} \quad A(r) = 2p \int_{r_{in}}^{r_0} r\ ds \tag{21}$$

Where:

$$ds = \sqrt{1 + \left(\frac{dz}{dr}\right)^2}\ dr \quad \text{and (17) becomes:} \quad \frac{dz}{dr} = \frac{\Omega^2}{g} r$$

Substituting and integrating:

$$A(r) = 2p \cdot \frac{g^2}{3\Omega^4} \cdot \left[\left(1 + \frac{\Omega^4}{g^2} r^2\right)^{\frac{3}{2}} - \left(1 + \frac{\Omega^4}{g^2} r_{in}^2\right)^{\frac{3}{2}} \right] \tag{22}$$

The parabolic area factor $PF_{area} = \frac{A(r_0)}{A_0}$ is the ratio of the new water surface area to the area of the surface without rotation and is obtained by substituting $r = r_0$ and $\Omega = \frac{V_w}{R_D}$ in equation (22) so: .

$$PF_{area} = \frac{2p \cdot \frac{g^2}{3\Omega^4} \cdot \left[\left(1 + \frac{\Omega^4}{g^2} r_0^2 \right)^{\frac{3}{2}} - \left(1 + \frac{\Omega^4}{g^2} r_{in}^2 \right)^{\frac{3}{2}} \right]}{p\left(r_0^2 - r_0^2 \right)} \quad (23)$$

After substituting the apparatus dimensions and simplifying, the parabolic area factor become:

$$PF_{area} = 8.879 \frac{\cdot \left[\left(1 + 0.11578\, V_w^4 \right)^{\frac{3}{2}} - \left(1 + 0.0407\, V_w^4 \right)^{\frac{3}{2}} \right]}{V_w^4} \quad (24)$$

where V_w is the water velocity in m s^{-1}. The increase in surface area due to rotation of the water will be used to obtain the exchange rates per unit surface area.

Similarly, an analysis has been made to define a parabolic torque correction factor for the shear stress that propels the rotational water motion. The basic assumption is that the shear stress over the water surface is not a function of the distance from the tank center or that $t_s \neq t_s(r)$. However, since the shear stress now is over a parabolic surface, let's denote the stress as t_{pf} (where the pf stand for parabolic factor). The stress t_{pf} acts on a differential surface area $2p\ r \cdot ds$ and the differential torque generated by the stress at a radial distance r is:

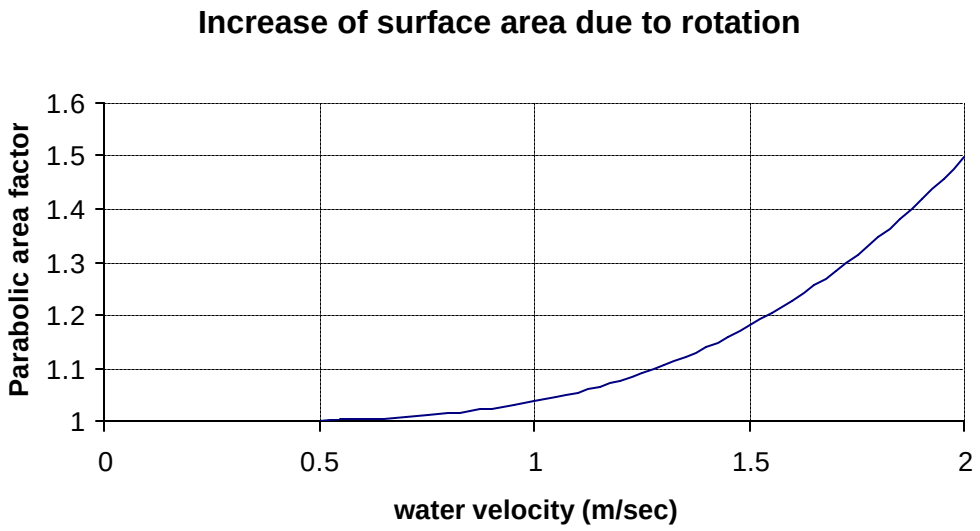

Figure 5: The ratio of the surface area due to rotation to the surface area without rotation as a function of the water velocity at the sonic Doppler location.

$$dT_{pf} = t_{pf}(2p\ rds)r = t_{pf}\,2p\ r^2 ds = t_{pf}\,2p\ r^2\sqrt{1+\left(\frac{dz}{dr}\right)^2}\ dr \qquad (25)$$

The solutions for t_{pf} becomes (Alamaro 2001):

$$t_{pf} = \left[\frac{\frac{2}{3}p\left(r_0^3 - r_{in}^3\right)}{2p\int_{r_{in}}^{r_0} r^2\sqrt{1+\left(\frac{V_w^4}{R_D^4 g^2}\right)r^2}\ dr}\right]\cdot t_s = \frac{t_s}{PF_{torque}} \qquad (26)$$

In equation (26) the term in the bracket is a correction factor for the shear stress over a parabolic water surface. Substituting the actual values for the apparatus dimensions r_0, r_{in}, R_D, and g we get:

$$PF_{torque} = 34.48 \int_{r_{in}}^{r_{out}} r^2 \sqrt{1 + 0.504\, V_w^4\, r^2}\; dr \qquad (27)$$

The explicit expression for the solution of equation (27) is a long and cumbersome expression. Therefore, the integral in (27) has been solved numerically for $0 < V_w < 2 \;\; m/\mathbf{sec}$. Curve fitting has been performed with a sixth degree polynomial to obtain a working formula for the torque parabolic factor as a function of the water velocity.

The shear stress for the rotating water mass in the wind wave tank is obtained by combining equations (16) and (27) and by using the dimensions of the tank to obtain:

$$t_{pf} = \frac{-1050 \cdot H \cdot \dfrac{\partial V_w}{\partial t}}{PF_{torque}} \qquad (28)$$

Where H is the water depth.

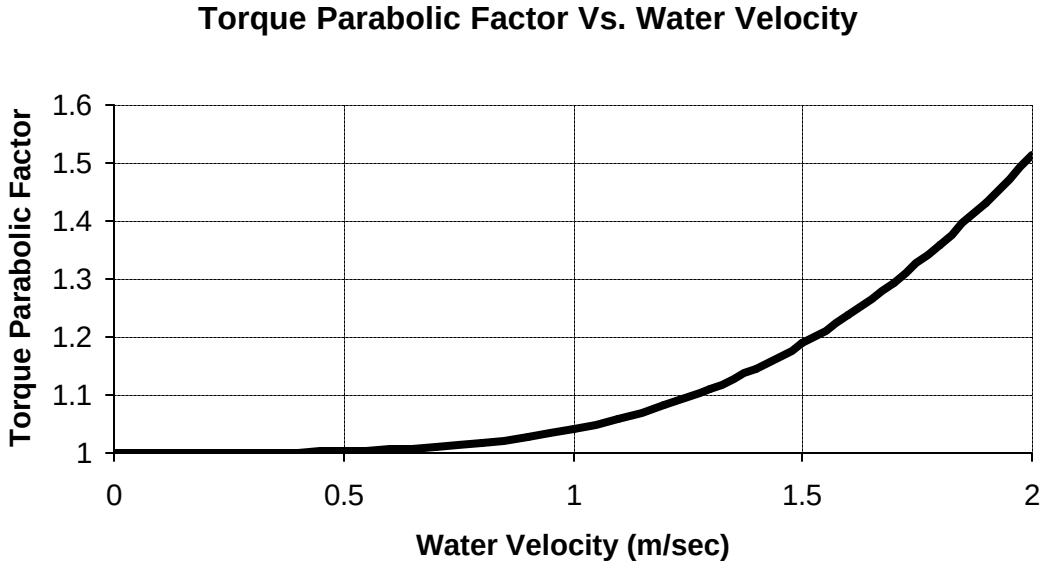

Figure 6: The correction factor to the propelling shear stress as a function of water velocity at the radial location of the ADV.

3. Fluid mechanics of rotational water and air and spindown experiments

3.1 Spindown formulation

The spindown technique is at the heart of this investigation. It provides information on the deceleration of the water mass that, in turn, enables the calculation of the shear stress over the water surface due to the airflow. The complexity of the experiment is mainly due to the surface waves and inertial oscillations that cause irregular tangential velocity. Ekman flows of both the water and the air also contribute to the flow irregularity. Other factors that contribute to uncertainty are due to instrument noise.

We hypothesize that the water flow in the tank can be modeled as a channel flow. This flow has a velocity V_w on the order of 0.5 m/sec, and hydraulic diameter D_h on the order of 0.2 m. Therefore, the Reynolds number of the water flow is about:

$$R_e = \frac{V_w D_h}{n_w} = \frac{0.5 \cdot 0.2}{10^{-6}} \approx 10^5 \tag{29}$$

Therefore, we expect the flow to be turbulent.

For turbulent and laminar channel (or pipe) flows, the friction factor f is always a decreasing function of R_e. This is shown graphically by the Moody Chart (Fox, 1998). Semi empirical formulas provide correlations for $f(R_e)$ for various ranges of R_e. For example, the Blasius correlation gives (Fox, 1998):

$$f = 4C_f = \frac{0.316}{R_e^{0.25}} \qquad \text{for } R_e \le 10^5 \tag{30}$$

Here C_f is the C_{DW} that we use for the drag that slows down the water during the spindown experiment due to the retarding shear stress over the tank walls. This is not the drag coefficient between the water surface and the airflow. According to the Moody Chart and the Blasius

correlation, for turbulent or laminar flow, C_{DW} is a decreasing function of R_e for all values of R_e.

The ODE describing the spindown is:

$$\frac{\partial V_w}{\partial t} = -Ar_w C_{DW}(R_e) V_w^2 = -k_1 C_{DW}(R_e) V_w^2 \quad (31)$$

where A is the wet wall area, r_w is the water density and k_1 is a constant for a specific experiment.

Assume that for a turbulent flow, C_{DW} is a power function of the Reynolds number, or equivalently, a power function of the water velocity:

$$C_{DW} \propto R_e^x \propto V_w^x \quad (32)$$

where x is any number.

Substituting (32) into (31);

$$\frac{\partial V_w}{\partial t} = -k V_w^{2+x} \quad (33)$$

Solving the last ODE:

$$V_w(t) = \frac{V_m}{(1+k \cdot t)^{\frac{1}{1+x}}} = \frac{V_m}{(1+k \cdot t)^n} \quad (34)$$

Where $n = \frac{1}{1+x}$, V_m is the water velocity at $t = 0$ and k is some constant. Also:

$$x = \frac{1-n}{n} \tag{35}$$

For x to be negative as required by the Blasius correlation or by the Moody Chart, it is required that:

$$n > 1 \tag{36}$$

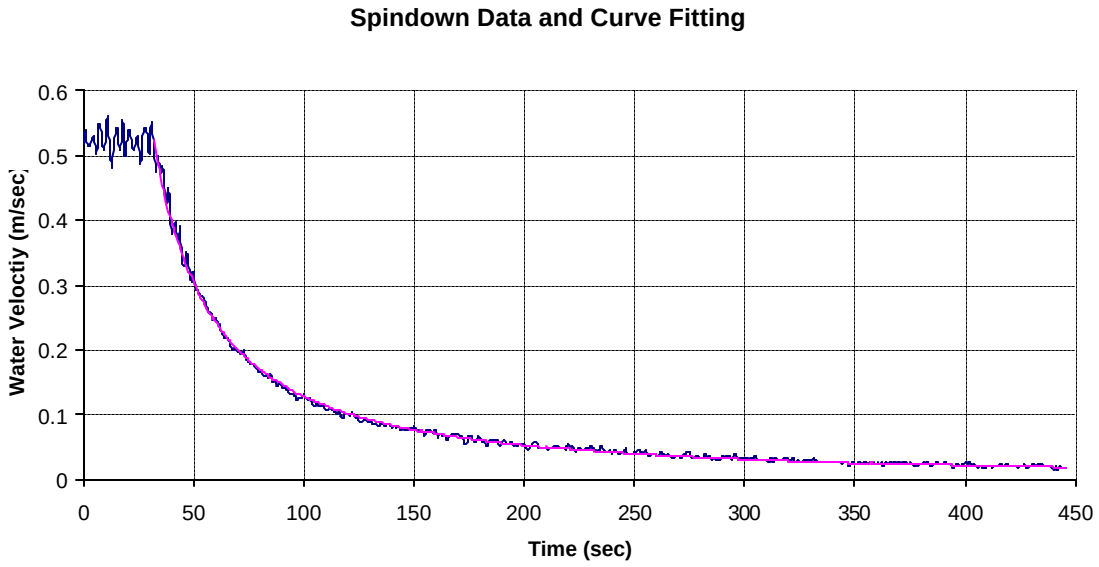

Figure 7: Spindown date and curve fitting

Figure 7 shows a spindown data and a curve fitting. For this particular experiment, the curve fitting gives:

$$V_w(t) = \frac{0.5222}{(1+0.0028562*t)^{1.3014}} \tag{37}$$

In eq. (37) $t = 0$ is the beginning of the spindown shown in Figure 7. Repeating the same spindown experiment a few times, different pairs of n and k are obtained simultaneously for each experiment.

3.2 The Derivative of water velocity

Once a curve fitting formula that has unique values of n and k is obtained for each spindown experiment, its time derivative is used to calculate of the shear stress using equation (29). The general form of the curve fitting formula is:

$$V_w(t) = \frac{V_m}{(1 + k \cdot t)^n} \tag{38}$$

Differentiation gives:

$$\frac{\partial V_w}{\partial t} = \frac{-nkV_m}{(1 + k \cdot t)^{n+1}} = \frac{-nkV_w}{(1 + k \cdot t)} = -nkV_w\left(\frac{V_w}{V_m}\right)^{\frac{1}{n}} \tag{39}$$

This expression has been used in (29) to calculate the shear stress.

3.3 Ekman Flows of the Water and Air

The water velocity in the boundary layer near the bottom of the tank is reduced. There, the radial pressure gradient is greater than the centrifugal force resulting in an inward motion of the water near the tank bottom.

Near the tank bottom there is, in addition to the tangential velocity, a velocity component in the radial direction toward the tank center. The water is upwelling near the inner wall and on the water surface the water motion spirals outward as shown in Figure 8. As for the air motion, for a tank covered with a lid, the air spirals inward near the water surface as shown in Figure 8. Near the inner wall, air is upwelling and it is possible that this upwelling air assists the upwelling of the water spray in high air speeds.

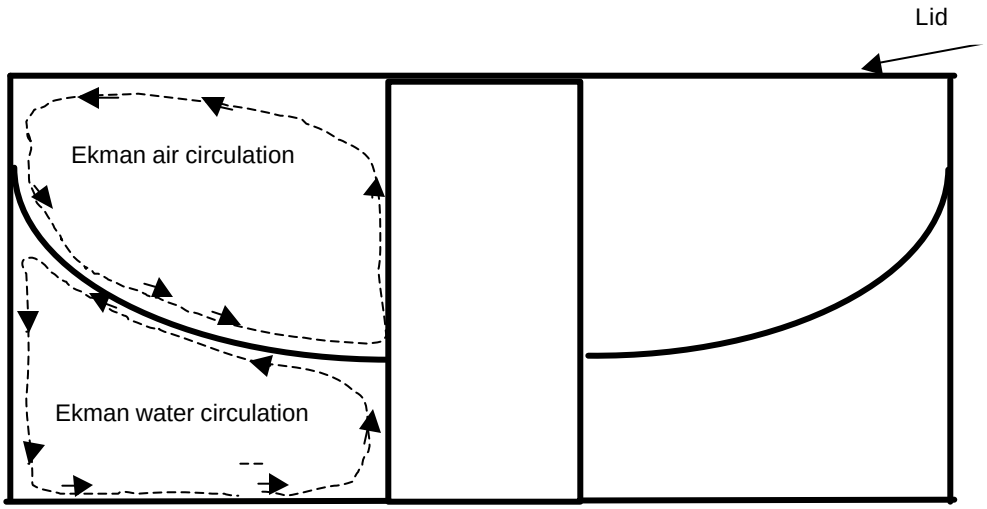

Figure 8: Ekman circulation of water and air in the radial direction. The air circulates as shown for a tank covered with a lid.

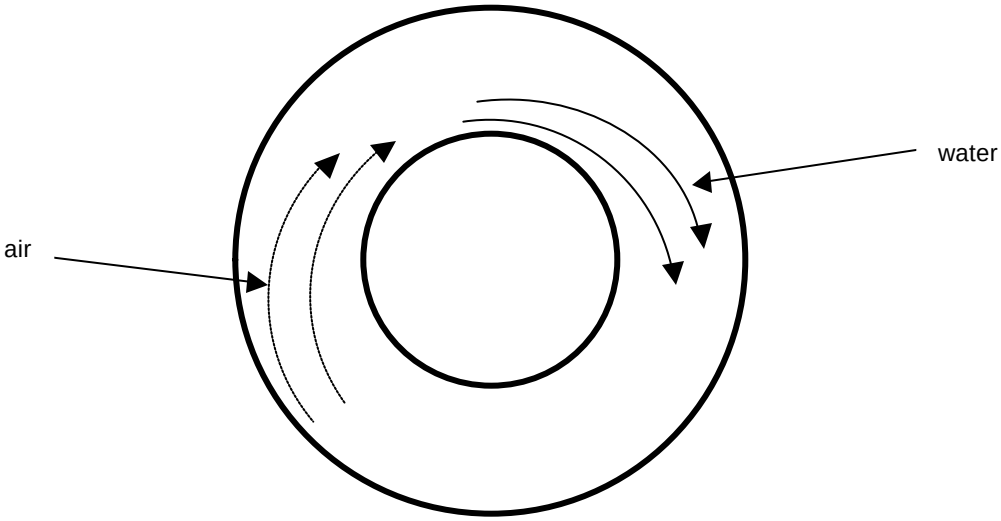

Figure 9: Upper view of the spiral flows of water and air near the water surface

It has been observed during the spindown that the abrupt cessation of the torque causes inertial oscillations and the radial water flow become unstable. The radial velocity occupies a larger cross section area by an order of magnitude than the cross section area for the tangential

velocity. Therefore, due to mass conservation, the radial oscillations and perturbations are amplified and cause substantial perturbations in the measured tangential water velocity.

4. A procedure for drag experiments, analysis and results

This section outlines, step-by-step, the procedure for the drag experiments, their analysis and results for drag coefficients. The following figures are shown for experiments that used a 14 cm water depth since for this water amount the ADV could measure the water velocity in the middle of the water column. Also, this depth of water was not so great as to reduce the maximum RPM for the given electric motor power. Experiments were done once with the lid on to enable high RPM and air speed and once with lid off to enable evaporation and enthalpy transfer from the tank to the ambient laboratory. The lid-off drag experiments reached a maximum RPM of 560 while the lid-off enthalpy experiments reached a maximum of 480 RPM. The lid-on drag experiments, however, reached 760 RPM. This is because, without the lid, the electric motor must not only do work against frictional dissipation in the apparatus, but must also accelerate ambient air that is continually exchanged through the top. Also, in the evaporation experiments, heating elements were submerged in the water, obstructing its flow and causing the maximum RPM to be lower than in the tank without heating elements.

a. The steady-state water velocity is measured vs. paddle RPM. The lowest RPM is 40 and the highest for a tank covered with a lid is about 760, depending on the amount of water in the tank. The RPM was changed by increments of 20. At low RPM, the time necessary to bring the water to steady state is long and it is generally shorter for higher RPM. For an intermediate 200-400 RPM, the necessary time is about 2 minutes. For the lowest 40 RPM the time can be as long as 7-10 minutes.

b. Once the water velocity reaches steady state, the water velocity is recorded for 30-60 seconds and is averaged for each RPM.

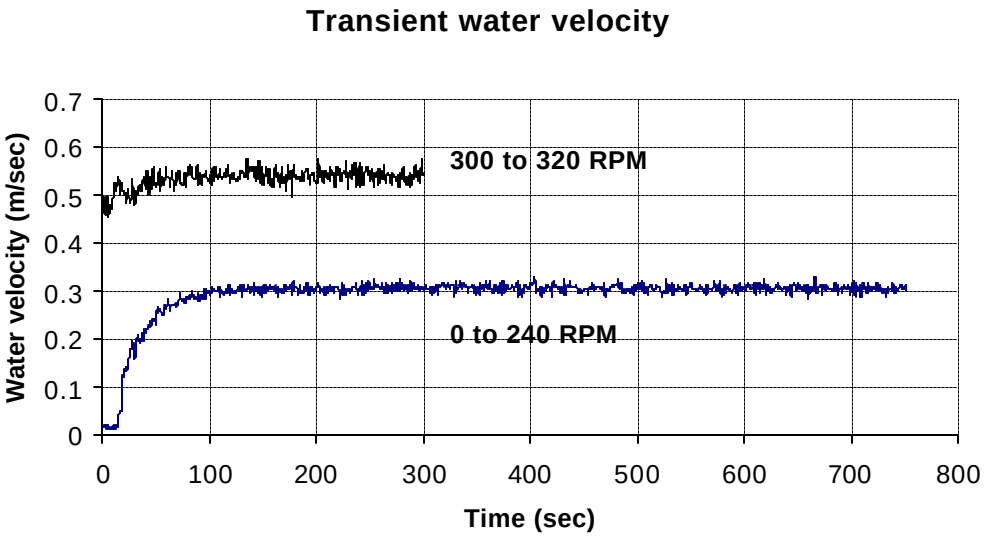

Figure 10: Time series of water velocity for RPM changes. The time necessary to bring the water to steady-state velocity is approximately 100 seconds

c. Air speed is measured as a function of RPM by an anemometer at a fixed height above the water surface and is shown in figure 12. The water speed for a specific RPM is subtracted from the air speed to obtain the relative air velocity over the water surface. Since relative air speed is known as a function of RPM and all other data is given as a function of RPM, all other data can

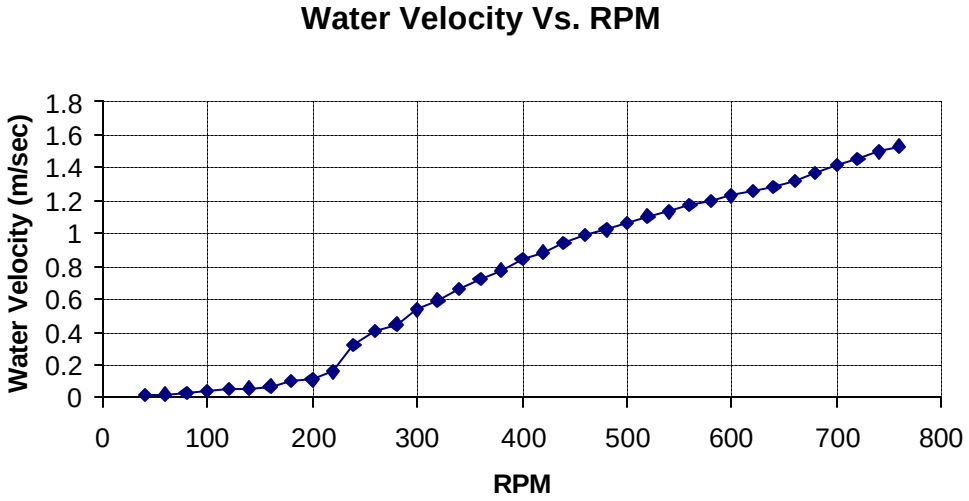

Figure 11: Water velocity vs. RPM. Around 220-280 RPM the surface becomes rough, resulting in wave drag and a marked increase in the slope of water velocity vs. RPM.

be calculated as a function of relative air speed. It was observed that the air speed strongly affects the water speed and wave pattern but water depth, speed and wave patterns do not significantly affect the air speed.

d. The spindown and curve fitting procedure described in section 3 is performed in order to calculate the n and k of the decelerating water velocity vs. time given by eq. (38). Once the curve fitting is performed, the best values of n and k are found. Their values are used in eq. (39) to calculate the time derivative of the velocity:

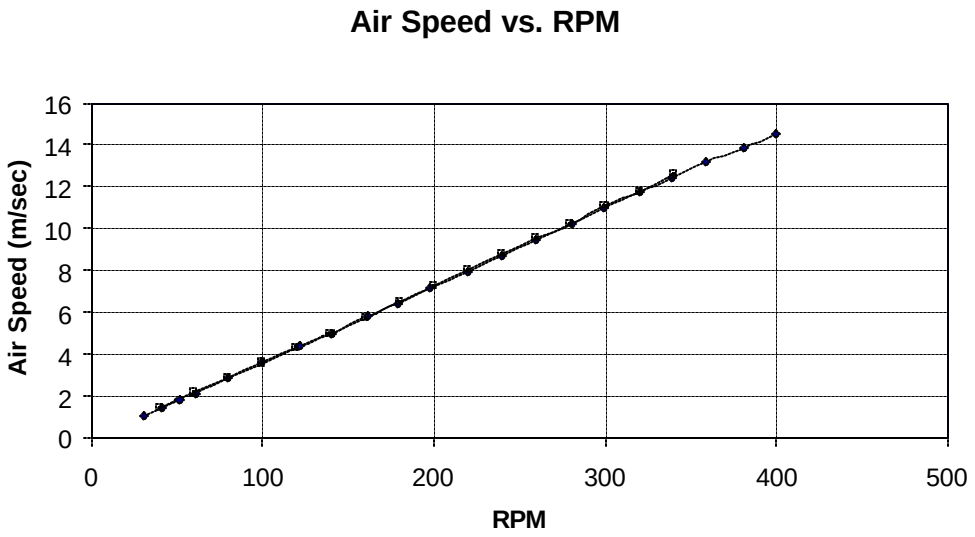

Figure 12: Air speed vs. RPM for two experiments. The water surface in the first is 25 cm and in the second is 12 cm above tank bottom. The air speed vs. RPM is approximately equal for the two experiments.

The derivative is used in eq. (28) to calculate the shear stress t_{pf} over the parabolic water surface. The friction velocity is obtained using:

$$u_* = \sqrt{\frac{t_{pf}}{r_a}} \tag{40}$$

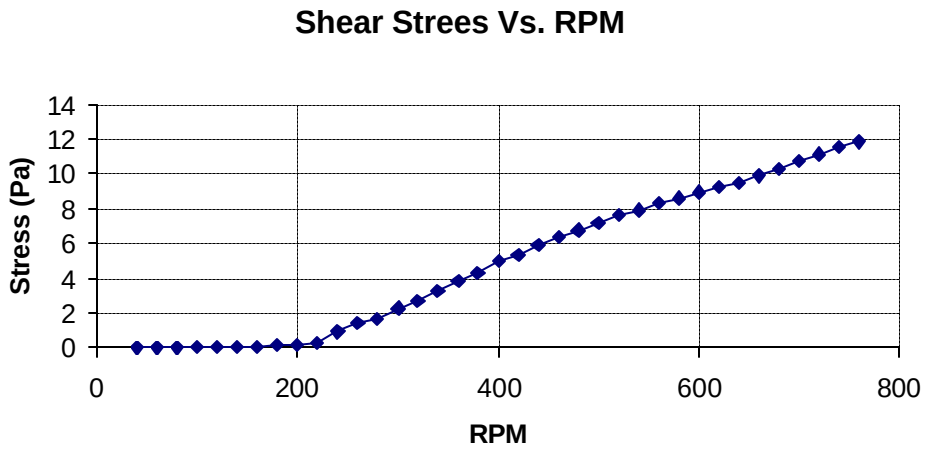

Figure 13: Typical Shear stress vs. RPM

where r_a is the air density.

The drag coefficient is calculated using the assumption that the wind velocity has a logarithmic profile and the wind speed at 10 m height is found by extrapolation. An intermediate step is the calculation of the "roughness" of the water surface. The expression for the roughness is:

$$\frac{u_a}{u_*} = \frac{1}{k}\ln\left(\frac{z_a}{z_0}\right) \tag{41}$$

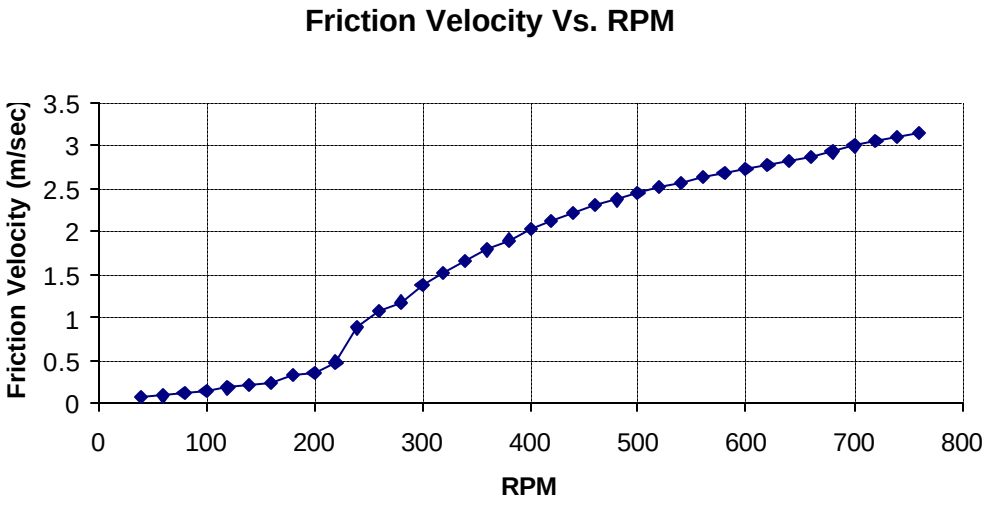

Figure 14: Typical friction velocity vs. RPM

where u_a is the relative air velocity over the water surface, measured at height z_a, and $k = 0.41$ is the Von Karman coefficient. The anemometer was placed at $0.425\ m$ above the tank bottom where the water surface height measured from the bottom of the tank is H, the expression for z_a is:

$$z_a = 0.425 - H \tag{42}$$

(41) enables the calculation of the roughness z_0:

$$z_0 = z_a \cdot \exp\left(-k\frac{u_a}{u_*}\right) \tag{43}$$

The air velocity at a height of 10 m above the water surface is found by re-arranging equation (41):

$$U_{10} = \frac{u_*}{k}\ln\left(\frac{10}{z_0}\right) \tag{44}$$

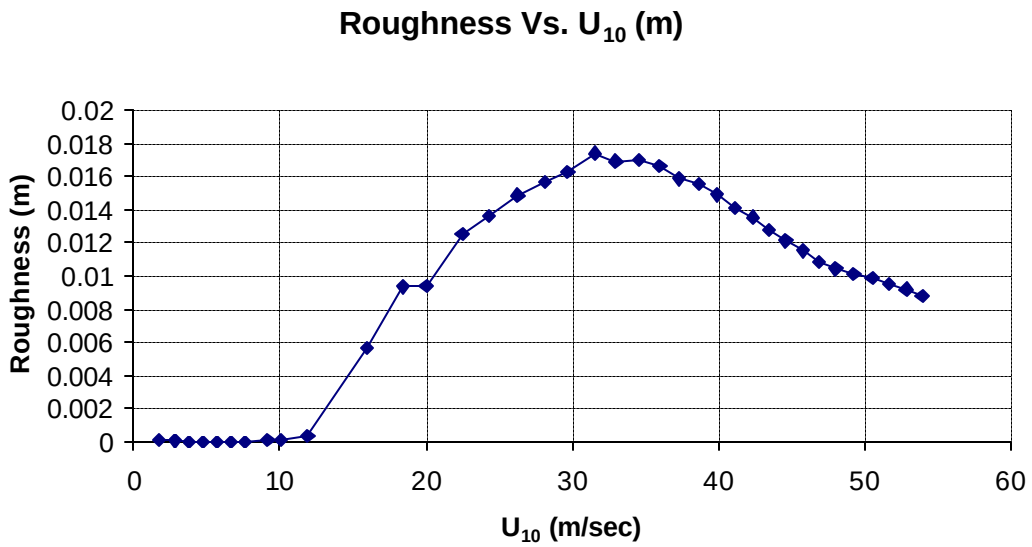

Figure 15: Roughness length in meters vs. U_{10}, the extrapolated air speed 10 meters above the water surface. The calculated "unphysical" roughness length range is 0-20 mm.

The non-dimensional drag coefficient is obtained by dividing the shear stress by the dynamic

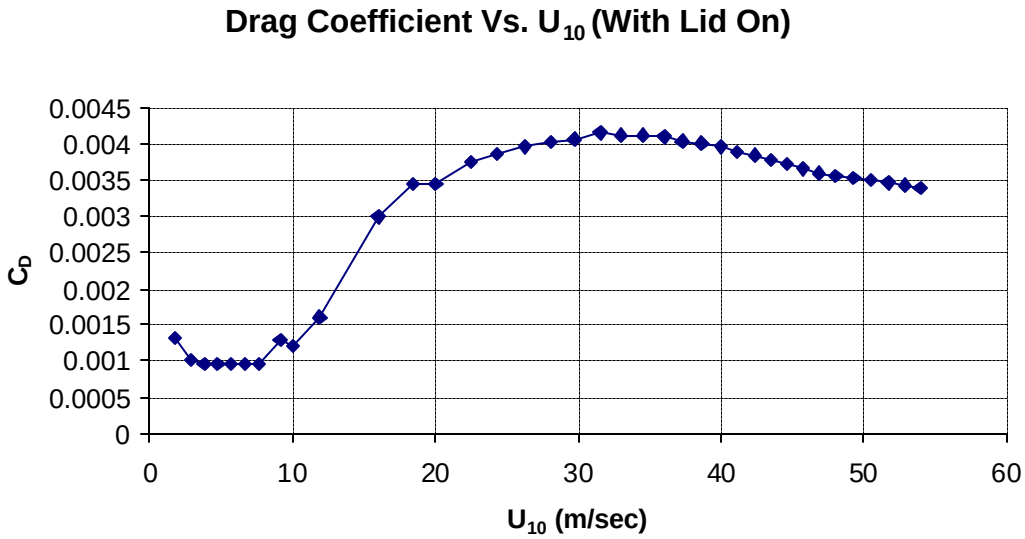

Figure 16: Drag coefficient vs. the extrapolated wind speed at a height of 10 meters above the water surface.

pressure at the reference air velocity U_{10} obtained in (44). The drag coefficient is:

$$C_D = \frac{t_s}{r_a U_{10}^2} = \left(\frac{u_*}{U_{10}} \right)^2 \qquad (45)$$

The enthalpy transfer experiments outlined in later sections were done with the lid off. Therefore, another set of drag experiments has been performed with the lid off in which the maximum RPM and the corresponding U_{10} was about 35 m s^{-1}.

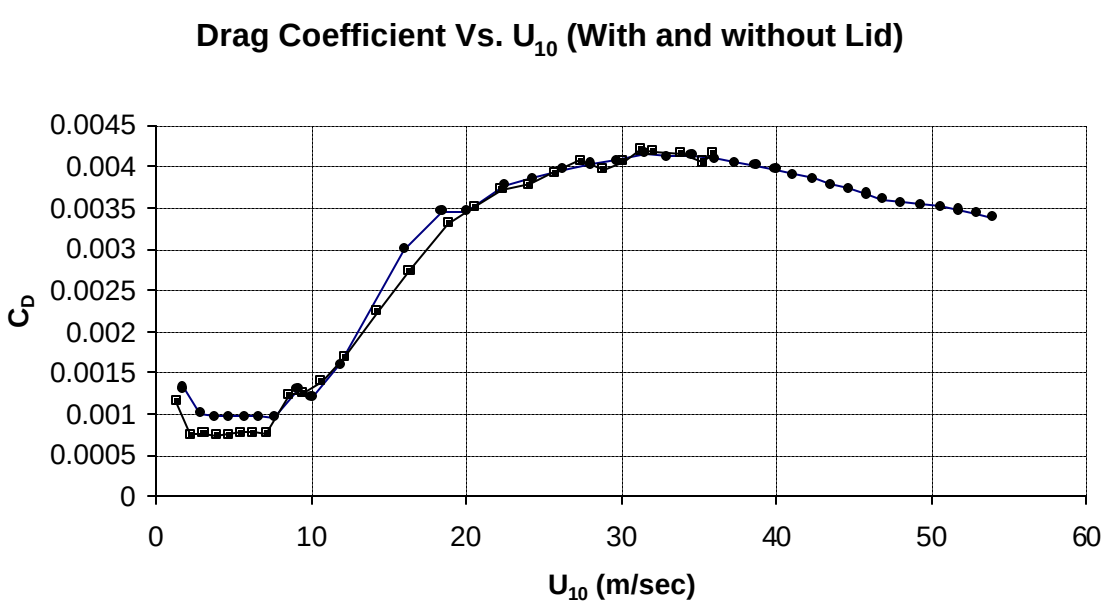

Figure 17: Drag coefficients Vs. U_{10} for with and without lid. The maximum U_{10} for with lid on is 35 m/sec. ● With lid on. ■ With lid off.

5. Enthalpy Transfer Experiments

5.1 Introduction and Experimental Apparatus

A schematic drawing for the tank equipped and modified for the enthalpy transfer experiment is shown in figure 19. Submerged heating elements are powered using a 20 Volt transformer. During the experiments, the paddle moves the air over the water. The air motion enhances the enthalpy transfer from the water into the lab ambient environment. Humidity and temperature sensors are placed in the room and this information is fed into a Program Logic Controller (PLC). A thermocouple measures the bulk temperature of the water in the tank and this information is also fed into the PLC. The PLC controls the on-off power input into the heating elements so the water temperature is kept equal (within a margin of 0.2 C) to the lab ambient temperature. In this way, heat transfer from the room into the tank is minimized.

The water level in the tank during all the enthalpy transfer experiments was 14 cm. This water height which was used for the drag experiments gave consistently results. Each experiment was conducted using Poland Springs™ water and the water was always changed after each experiment. Each experiment was conducted over 24-48 hours. The surface tension of the

water was measured before and after an experiment. It did not change, having a value of 75-80 dyne/cm.

The water in the tank is connected by a pipe to an external cup so the water levels in the tank and the cup are equal. A needle attached to a micrometer is used to gauge the water level in the cup before and after the experiment, measuring the water loss during the experiment. The water level in the tank during the experiment was kept at $14 \pm 1\,cm$. If necessary, the experiment was briefly interrupted and a known amount of water was added. Each experiment was done for a specific RPM. Air velocity vs. RPM was measured using an anemometer at a specified height above the water surface, as in the drag experiments.

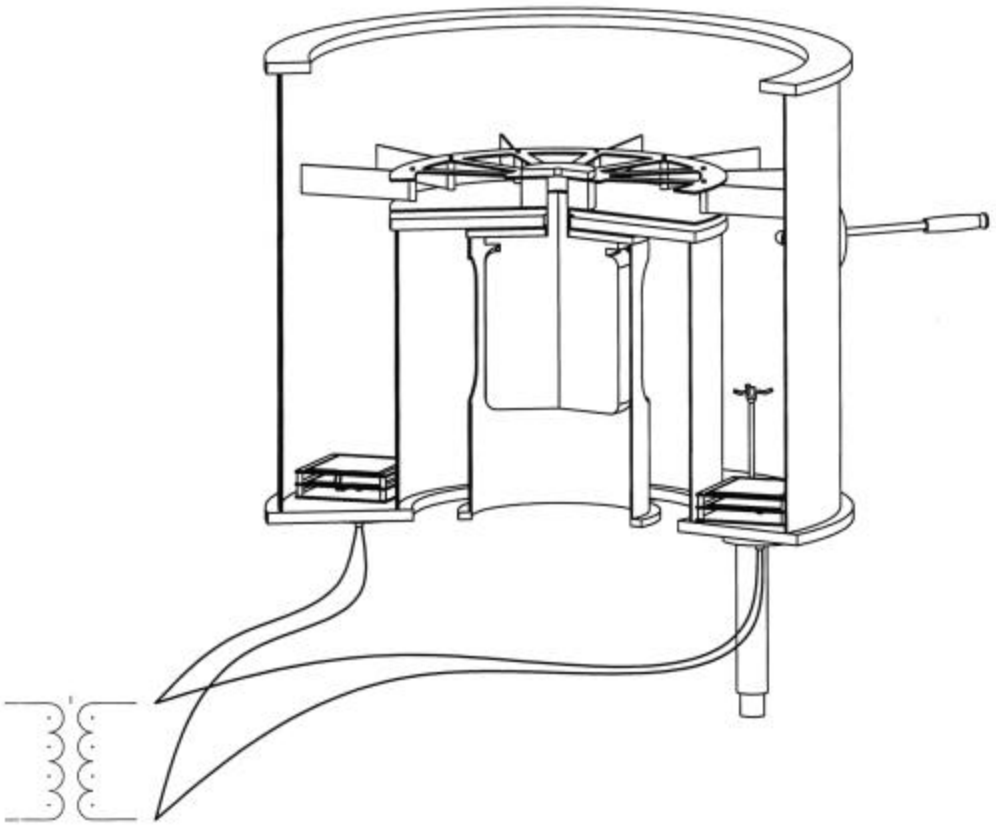

Figure 18: Wind wave tank equipped with heating elements

The electric motor has an efficiency of less than 100% in converting electric power to shaft power. Therefore, the motor tends to release heat conducted through the motor case, which was leaking into the surrounding water. To solve this, a fan was installed in a duct. The fan causes air at room temperature to enter the annulus surrounding the electric motor. The cold air flows upward and is expelled warmer downward, preventing heat from leaking into the water.

5.2 Latent Enthalpy Transfer

The following formulation and analysis shows that for an experiment in which the water and the ambient temperature are equal, the latent enthalpy transfer and the mass transfer coefficients are also equal.

The latent enthalpy transfer from the water is:

$$\dot{m}L_{V,w} = C_K V_a A\left(\rho_{sat,w} L_{V,w} - \phi\ \rho_{sat,air} L_{V,air}\right) \tag{46}$$

where $\dot{m}$ is the mass rate of evaporation, $L_{V,w}$ is the latent heat of evaporation at the temperature of the water, $L_{V,air}$ is the latent heat of evaporation at the temperature of the air, C_K is the enthalpy transfer coefficient, V_a is the air velocity, A is the water surface area, ϕ is the relative humidity, and $\rho_{sat,w}$ and $\rho_{sat,air}$ are the saturation water vapor density at the water and air temperature respectively.

Because, in our experimental setting, the heating elements keep the water temperature equal to the air temperature, $L_{V,w} = L_{V,air}$ and $\rho_{sat,w} = \rho_{sat,air}$. Therefore, eq. (46) is reduced to give:

$$\dot{m} = C_K V_a A \rho_{sat,w}\left(1-\phi\right) \tag{47}$$

or

$$C_K = \frac{\dot{m}}{V_a A \rho_{sat,w}\left(1-\phi\right)} \tag{48}$$

The last expression for C_K - the enthalpy transfer coefficient - is equivalent to the mass transfer coefficient for these specific experimental conditions.

Eq. (47) can also be written as $\frac{dm}{dt} = C_K V_a A r_{sat,w}(1-f\ )$. Integrating:

$$\int_0^{m_{tot}} dm = m_{tot} = C_K V_a A \int_0^T r_{sat,w}(1-f\ )dt \tag{49}$$

or

$$C_K = \frac{m_{tot}}{V_a A \int_0^T r_{sat,w}(1-f\ )dt} \tag{50}$$

where m_{tot} is the total water mass evaporated in a specific experiment. In our procedure, each experiment lasts $n = 1{,}000 - 2{,}000\ \mathbf{min}$, and $r_{sat,w} = r_{sat,w}(t)$ and $f = f(t)$. The temperature and relative humidity (RH) are recorded once per minute.

The integral in (50) is performed numerically to give:

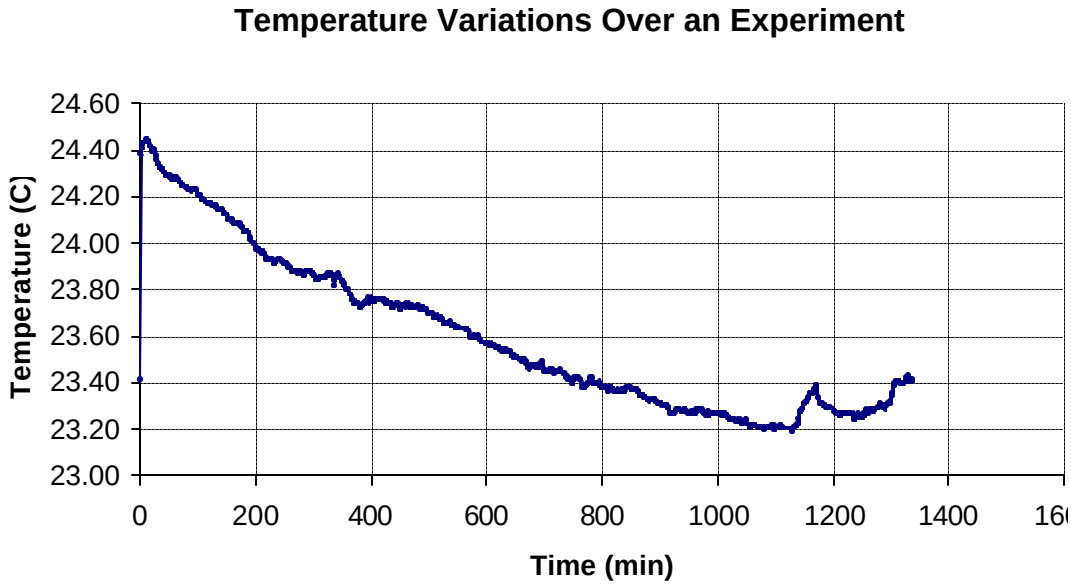

Figure 19: Typical temperature variations over an enthalpy transfer experiment

$$C_K = \frac{m_{tot}}{V_a A \sum_1^n r_{sat,wi}\left(1 - f_i\right)\Delta t} \tag{51}$$

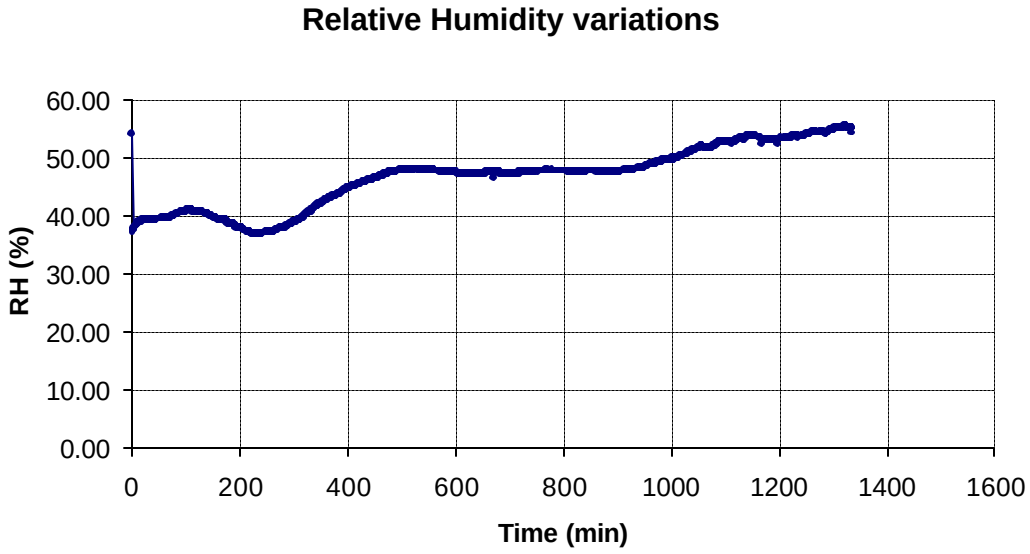

Figure 20: Typical relative humidity variation over an enthalpy transfer experiment

In fact, since the heating elements are activated by a temperature difference between the ambient air and water, there are slight temperature differences between the water and room temperature of about 0.3 C on average. Therefore, eq. (51) may be re-written more accurately as:

$$C_K = \frac{m_{tot}}{V_a A \Delta t \sum_1^n \left(r_{sat,wi} - f_i r_{sat,air,i}\right)} \tag{52}$$

Since the tank walls are not perfectly circular, the cross sectional area of the tank was measured around the height of the water surface using a known amount of water and measuring its rise using the micrometer. The measured water surface area is $A = 0.4769\, m^2$. Using this and $\Delta t = 60\ \mathbf{sec}$ (data recording interval by the spreadsheet) in eq. (52), it becomes:

$$C_{K,latent} = 3.495\ 10^{-2}\ \frac{m_{tot}}{V_a \sum_{1}^{n} (r_{sat,wi} - f_i\, r_{sat,air,i})} \tag{53}$$

where m_{tot} is the total water mass evaporated in Kg during a specific experiment, V_a is the air speed in m s^{-1}, f_i is the relative humidity each minute. The saturation water vapor pressure at the water surface and in the air as a function of temperature is calculated using the semi-empirical Clausius-Clayperon equation (Ludlam, 1980):

$$P_s = 100\,\mathbf{exp}\left[1.8096 + \frac{17.27(T - 273.16)}{(T - 35.86)}\right] \tag{54}$$

where T is the temperature in K. The saturation vapor density is calculated using the ideal gas equation:

$$r_{sat} = \frac{P_s}{R_{H_2O} \cdot T} \tag{55}$$

Where R_{H_2O} is the gas constant for water vapor. $R_{H_2O} = 461.5 \frac{J}{Kg \cdot K}$.

Experiments were performed for 100, 120, 140…..480 RPM. The air velocity for each RPM was measured using the anemometer, and the temperature of the water, ambient air and relative humidity were recorded enabling the calculation of $\sum_{1}^{n} \left(r_{sat,wi} - f_i\, r_{sat,air,i}\right)$ for each experiment.

A summary of the latent enthalpy transfer coefficient Vs. V_{RPM} is shown in figure21. V_{RPM} is the air velocity at the height of the anemometer placement, 0.285 m above the water surface.

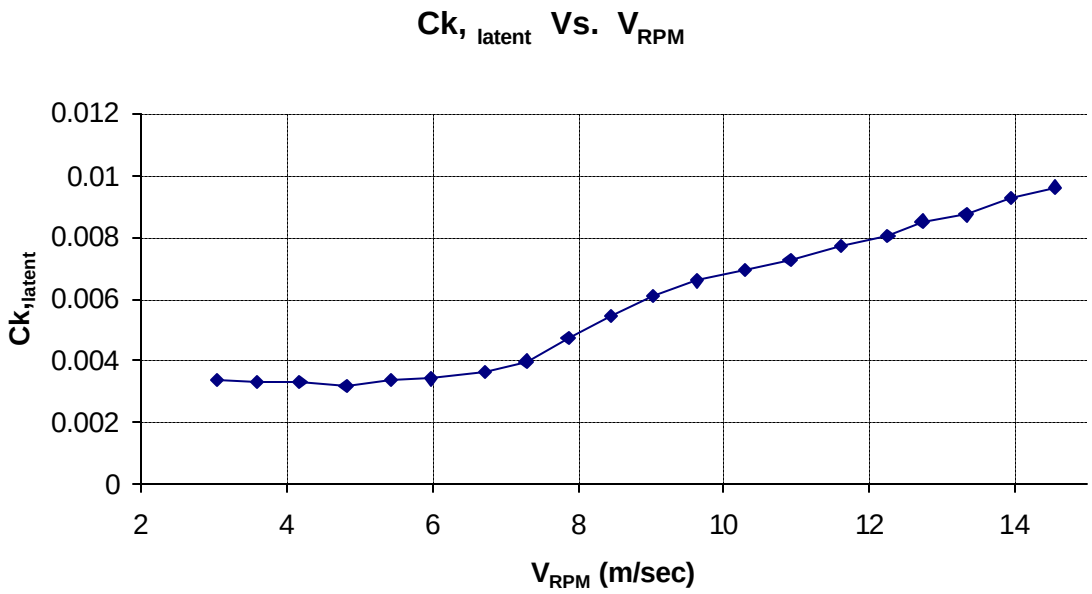

Figure 21: Latent enthalpy transfer coefficient $C_{k,\,latent}$ Vs. V_{RPM} - air velocity measured at 0.285 m above the water surface.

Later, these values of $C_{k,\,latent}$ will be revised using U_{10} instead of V_{RPM}.

5.3 Sensible and Total Enthalpy Transfers

Although the bulk temperature of the water during the experiment was kept equal to the temperature of the ambient air, there was sensible heat transfer from the ambient air into the water at all RPM.

The average power provided into the heating element was recorded once a minute. The power loss from the external wires leading to the heating elements was measured to be 3.9% of the total power provided by the transformer. For each RPM, the total energy was divided by the total evaporated water mass. This provides the "calculated heat of evaporation" denoted as $L_{V,C}$.

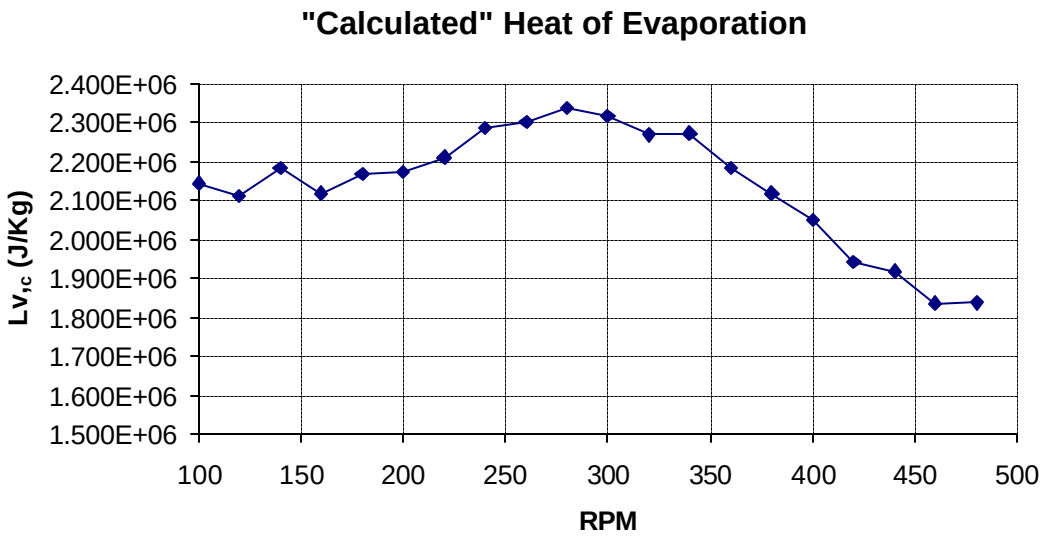

Figure 22: The "calculated" heat of evaporation. This is the total energy provided by the heating elements divided by total mass of water evaporated for a specific RPM of enthalpy transfer experiment.

Figure 22 shows that the heat provided by the heating elements is less than the specified heat of evaporation of water at the temperature range at which these experiments were done, which is 2.44 10^6 J/Kg. The temperature of the water during all the experiments was 23.5 ± 1.5 C introducing maximum error of no more than 0.15% in the value of the theoretical heat of evaporation. Therefore, since the values shown in Figure 23 are less than 2.44 10^6 J/Kg, it is clear that heat was leaking into the water assisting the heating elements in evaporating the water.

For low RPM, the water in the tank is not well mixed and is thermally stratified. In fact, a thin cold film was present on the surface of the water. This film cools the air in the tank just above the water. Owing to turbulence and Ekman flow, the cold air is transported out of the tank while warmer ambient air replaces it. The net result is heat transport into the tank.

At intermediate RPM, the water is well mixed so the bulk temperature of the water is closer to the temperature of the water surface. Therefore, the temperature of the air transported out of the tank is closer to the bulk temperature of the water and as a result, less heat is transported into the tank. As shown in figure 22, for the intermediate 200-300 RPM the calculated heat of

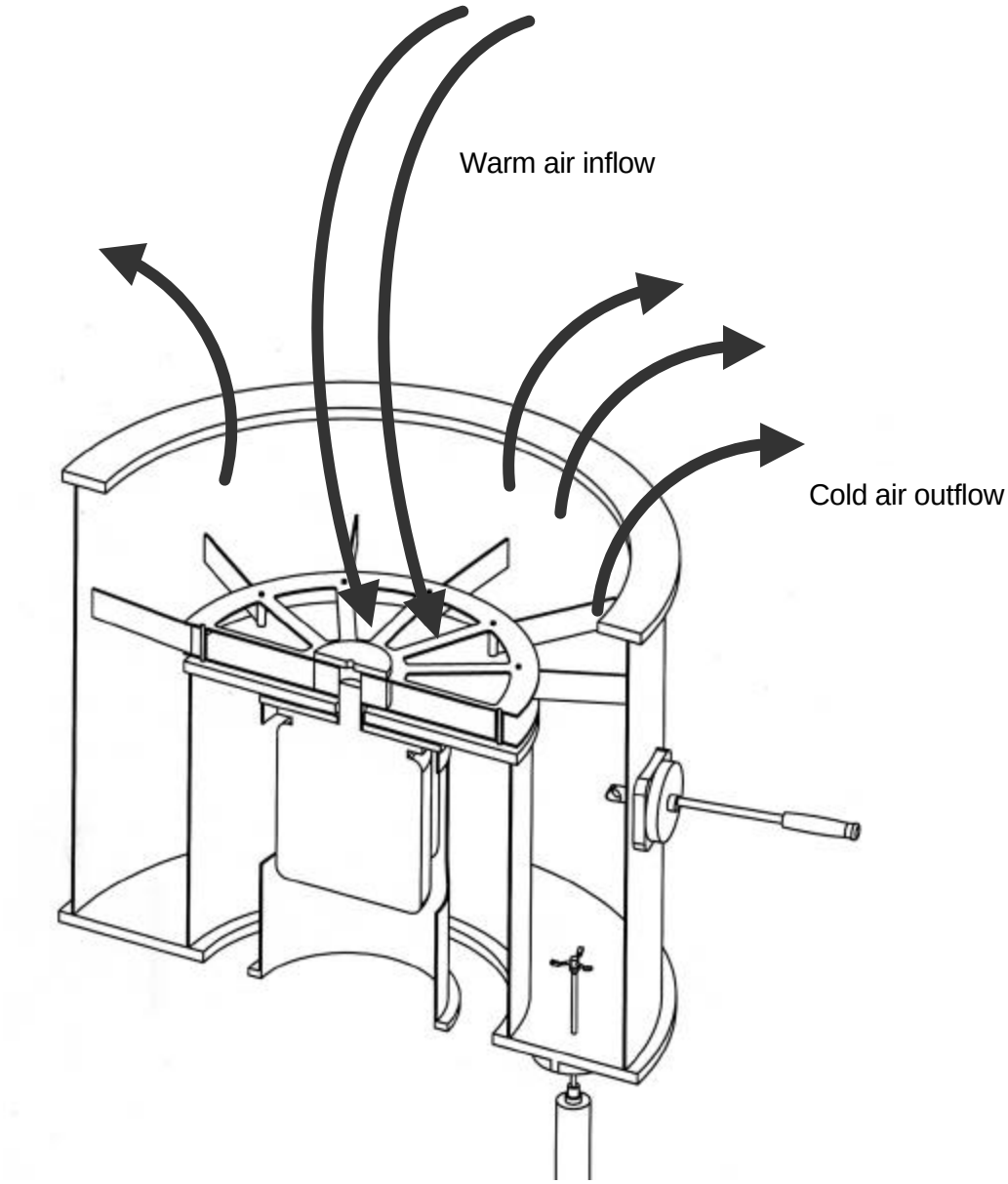

Figure 23: A schematic diagram of air flows into and out of the tank during evaporation experiments when the tank was not covered with a lid. Cold air is expelled out near the outer walls while warmer ambient air flows into the tank. The net result is heat transport into the tank.

evaporation reaches a maximum level, since at these RPM less sensible heat is transported into the tank, requiring more thermal energy from the heating elements. At high RPM, however, a spray is generated over the water surface, so the air over the water surface becomes moister and colder. This colder air is transported out of the tank and there is a substantial net heat

transport into the tank. It is quite possible that dissipation over the water surface at high RPM also contributed heat flow into the water. At 480 RPM, about 25% of the heat required for evaporation is provided by sensible heat transfer, while the rest is provided by the heating elements.

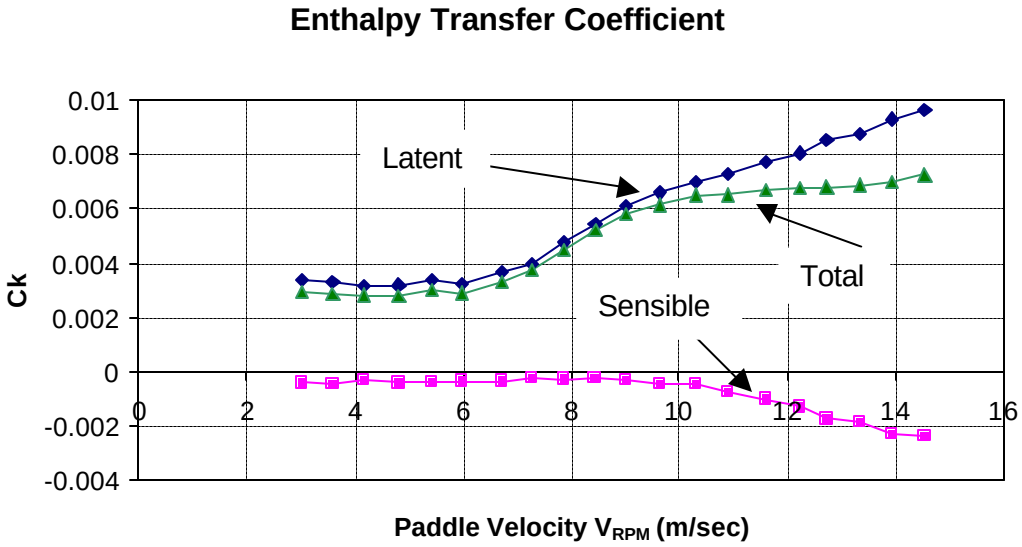

Figure 24: Latent, sensible and total enthalpy transfer coefficients vs. V_{RPM} - the air velocity in the tank. (The values given here are larger than the traditional values in the literature since usually these coefficients are non-dimensionalized using U_{10} as shown later).

The calculation of the sensible enthalpy transfer coefficient is straightforward. For each RPM, the "calculated heat of evaporation" $L_{V,C}$ was found and the difference between this value and the theoretical value for the heat of evaporation is a measure of the sensible portion of the enthalpy transfer coefficient, or:

$$C_{k,sensible} = C_{k,latent}\left(\frac{Lv,c - 2.4410^{6}}{2.4410^{6}}\right) \quad (56)$$

The sensible portion of the enthalpy transfer coefficient is negative since sensible heat is transferred into the water. The total enthalpy transfer coefficient is simply:

$$C_{k,total} = C_{k,latent} + C_{k,sensible} = C_{k,latent} \frac{Lv,c}{2.44\,10^{6}} \tag{57}$$

5.4 Comments on merging enthalpy and momentum transfer experimental data

In order to non-dimesionalize the enthalpy transfer coefficients using U_{10} instead the measured air speed V_{RPM} it is necessary to use the information on the shear stress and friction velocity for each experiment. The evaporation experiments were done with the tank lid off and heating elements immersed in the water. Proper drag experiment and their results for the enthalpy transfer coefficients should also use heating elements in the water and a tank without a lid.

We tried to use a new approach for measuring the drag. The electric motor that powers the paddle was placed on frictionless bearings. The torque provided to the paddle results in a reaction torque on the electric motor. A transducer was placed at a certain distance from the axis of the electric motor to measure the reaction force. This, at least in theory, enables measuring the torque provided on the paddle, which in turn enables calculating the shear stress and ultimately the drag coefficient. Furthermore, the torque together with the angular velocity of the paddle enables the calculation of the shaft power provided to the paddle, which is dissipated over the water surface.

The goal in using this approach was to find and calculate the drag due only to the water in the tank. Therefore, the torque was measured once with water in the tank and another set of experiments used a false bottom in the tank to account for the drag and resulting torque owing to the tank walls. In theory, measuring the torque with water in the tank and subtracting the torque when using a false bottom would provide the torque owing only to the water surface.

Unfortunately, the incremental torque due to the water in the tank in comparison to the torque with the false bottom is too small and, in fact, much smaller than the error in measuring the torque. Therefore, this approach was abandoned. The other possibility is to use spindown

experiments similar to those used before (Alamaro 2001). These spindown experiments may be used with heating elements in the water while the lid is off as was done in the enthalpy transfer experiments.

This approach has the following flaws. The spindown analysis used in the drag experiments earlier assumed that the water mass is at a rigid body rotation and, implicitly, the moment of inertia of the water mass was calculated. However, when heating elements are immersed in the water they introduce an obstruction that causes some of the water mass to barely move. It is impractical or impossible to estimate the moment of inertia of the water mass when heating elements are in the water.

Therefore, the following combined enthalpy and momentum transfer analysis uses the drag experiments described in earlier sections. This analysis interpolates to find C_D and U_{10} for each RPM used in the enthalpy transfer experiments.

5.5 *Computation of non-dimensional Transfer Coefficients using extrapolated* U_{10}

Figures 16 and 17 in section 5 provide the drag coefficient Vs. U_{10} up to $U_{10} \approx 55\ ms^{-1}$ for the tank covered with a lid, and up to $U_{10} \approx 35\ ms^{-1}$ for the tank without a lid. The

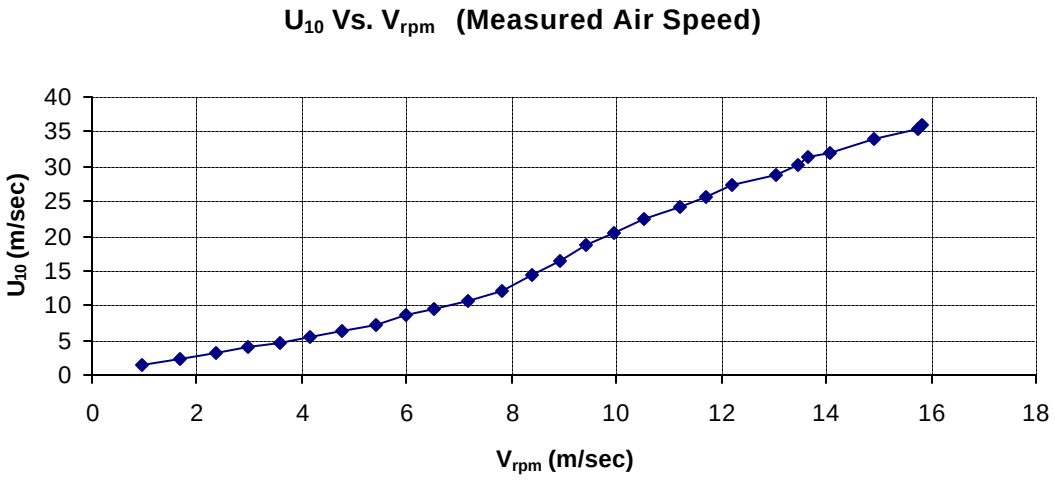

Figure 25: Extrapolated U_{10} Vs. measured air speed at 0.285 m above water surface.

results for drag experiments for the tank without the lid are used here to non-dimensionalize the enthalpy transfer coefficient using U_{10}, instead of the measured air speed in the tank.

The drag experiments did not use heating elements in the water and they were done once with the lid on and once with the lid off. Although the drag results with the lid on provide useful information, the drag experiments for the lid-off case were used to find the equivalent roughness, friction velocity and U_{10} that corresponds to each enthalpy transfer experiment. Figure 25 provides the U_{10} Vs. the measured air velocity in the tank when drag experiments were done with the lid off and without heating elements. As shown, at about $U_{10} \cong 12\ ms^{-1}$ there is a substantial increase in the slope owing to wave formation and associated roughness increase. For $U_{10} > 20\ ms^{-1}$ waves are attenuated and the slope is decreased.

The enthalpy transfer experiments, however, were done with the heating elements in the water. These obstructed the water flow and reduce the RPM. Linear interpolation was used to provide values for U_{10} and C_D for air speed that correspond to the enthalpy transfer experiments without heating elements.

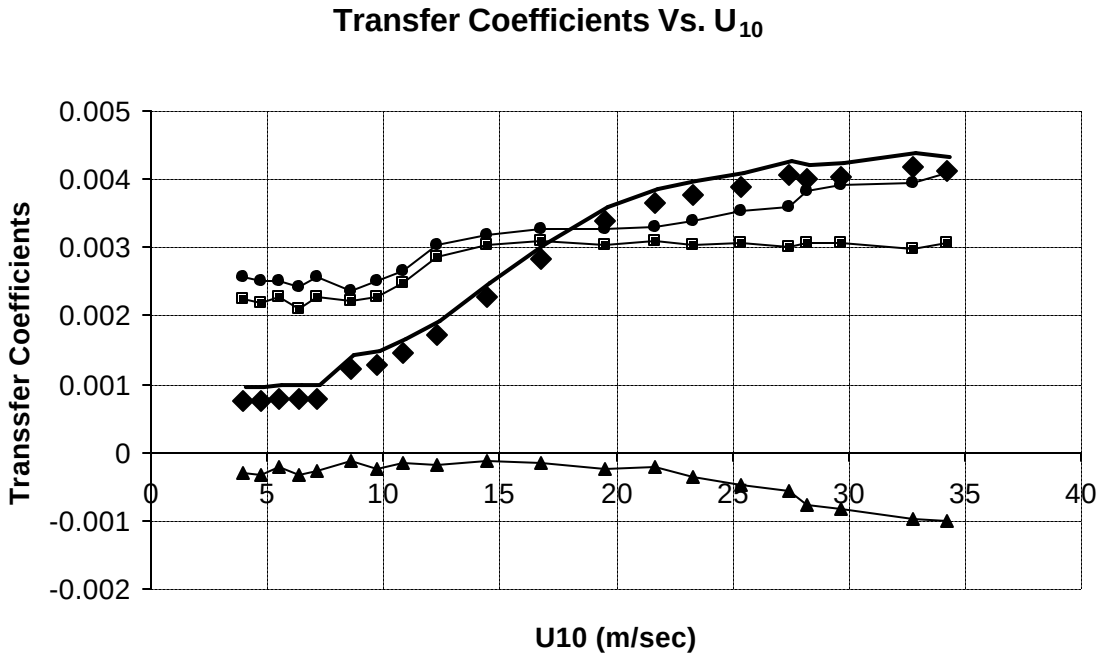

Figure 27: Enthalpy transfer coefficients Vs. U_{10} • Latent. ? Sensible. ■ Total. ◆ Drag.

6. Discussion and conclusions

The scientific goal of this experimental study is to determine the dependence of the drag and enthalpy transfer coefficients on wind speed. A comparison between characteristics of a few experiments was made. Such a comparison is important for identifying the limitations of the apparatus and to design future experiments.

The false bottom is a valuable component of the facility. It can be used to vary the distance from the paddle to the water surface without changing the amount of water in the tank. Unfortunately, the possible height changes implemented by the false bottom are no more than 20 cm owing to the height of the tank.

In further studies it might be useful to consider modifying the wind-wave tank by increasing its height to about 3-5 meters. In such a tank, the false bottom position could be changed by meters rather than centimeters. Also, a tall tank in which the paddle is much higher than the water surface will prevent the water spray from reaching the paddle blades.

.

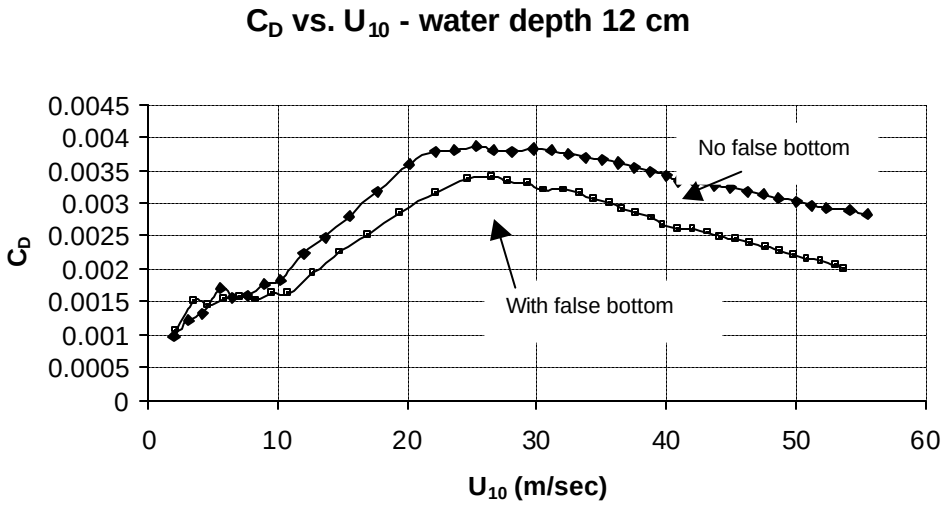

Figure 28: Drag coefficient vs. U_{10} for 12 cm water depth with and without false bottom. The false bottom is placed 13 cm above the tank bottom.

Numerous experiments were performed for water depths of 8, 10, 12, 14 and 16 cm using various elevations of the false bottom. The lowest water depth was 8 cm. It was found that for this depth, the ADV couldn't measure the water velocity in the middle of the water column as necessary. On the other hand, experiments with a 16 cm water depth could not reach high wind speed since the water moment of inertia is too high and the power of the electric motor is not enough to propel such a large amount of water. Future modifications of the tank should include a larger and more powerful motor.

At high RPM the water velocity reached 1.5 - 1.7 m/sec. Owing to the parabolic shape of the water surface, the distance from the water surface to the paddle near the outer wall is different from the distance near the inner wall. This difference can reach 15 cm for $V_w \cong 1.7\ m/\mathbf{sec}.$ This introduces an error in calculating z_a, the distance from the water surface to the paddle that is used in the calculation of U_{10}. The highly parabolic water surface for high RPM also alters the moment of inertia of the water mass, and this introduces an error in the calculation of the shear stress.

It was also observed that at a paddle RPM that corresponds to $U_{10} \cong 30\ m/\mathbf{sec}$ and higher, water spray is generated, especially when the lid is on. It is estimated that the centrifugal acceleration of the spray is on the order of $100-200\ m/\mathbf{sec}^2$ so that its flight time scale before impacting the tank walls is about 0.1 sec. This point may explain the declining C_D for $U_{10} > 25\ m/\mathbf{sec}$ and should be the subject of further investigation.

The enthalpy transfer experiments seem to provide useful and accurate information as far as the latent enthalpy transfer is concerned. However, the tank air inflow and outflow govern the sensible heat transfer, and this flow pattern in our experiment does not necessarily resemble conditions over the ocean. In addition, at high RPM, mechanical dissipation in the air above the water surface and on the tank walls might contribute to sensible heat transfer into the water. It seems, therefore, the obtained quantitative results for the sensible heat transfer probably are not representative of nature.

Acknowledgment:

The authors wish to thank the MIT Edgerly Fund for providing the funding for the wind wave tank construction and to Peter Morley and David Bono for their technical assistance.

References:

Alamaro, M.; "Wind Wave Tank for the Investigation of Momentum and Enthalpy Transfer from the Ocean Surface at High Wind Speed," Master thesis at the Department of Earth, Atmospheric and Planetary Sciences, Massachusetts Institute of May, 2001. See also: http://web.mit.edu/hurricanelab/ThesisWebsite.pdf

Bistre, M. and Emanuel, K.A., 1998: Dissipative heating and hurricane intensity. *Meteoric. Atoms*. Physic. **65**, 233-240.

Emanuel, K.A., 1986: An air-sea interaction theory for tropical cyclones. Part I. *J. Atmos. Sci.*, **42**, 1062-1071.

Emanuel, K.A., 1988: The maximum intensity of hurricanes. *J. Atmos. Sci.*, **45**, 1143-1155.

Fox, R.W, and McDonald, A.T. 1998: *Introduction to Fluid Mechanics*. John Wiley & Sons, Inc., New York.

Ludlam, F.H., "Clouds and storms; the behavior and effect of water in the atmosphere," The Pennsylvania State University Press, 1980.

DISCARD